Image Processing, Electronics and Computers
L. Trajkovic et al. (Eds.)

doi:10.3233/ATDE240462

Research on Fast Extraction of Soccer Robot Movement Trajectories Based on Improved Low-Rank Trajectory Recovery

Meiheng ZHANG[1]
Harbin Huade University, Harbin, China

Abstract. This paper presents a computer-assisted rapid trajectory extraction technique for soccer robots' global vision system, focusing on Low-Rank Trajectory Recovery (LRTR). This system is crucial for providing robot posture data, enhancing decision-making, robot trajectories, and maneuver strategies. Given the competition rules demanding quick onsite vision system setup and adjustment, this method offers a speedy and accurate extracction process. It aims to refine trajectory tracking precision in high-level soccer matches, especially by processing varied noisy images in real scenarios. The study delves into theoretical and practical aspects, highlighting its effectiveness in minimizing extraction errors amid the unpredictability of robot movement in competitions. Utilizing robust subspace learning within LRTR significantly enhances tracking accuracy, object recognition, and scene understanding. The innovative trajectory feature extraction method evaluated here shows considerable promise in efficacy and adaptability. The findings advance computer vision system development and improve trajectory interpretation for diverse applications, including sports tracking and autonomous systems. When compared to other algorithms, this method stands out for its extraction precision and efficiency in robot operation, achieving an impressive extraction accuracy of ±2.67 mm without specialized targets, showcasing superior performance.

Keywords. Soccer Robot, global vision system, camera extraction, Low-rank trajectory recovery, feature extraction

1. Introduction

Research in soccer robot systems is a key focus in robotics, categorized by their vision technology into global and individual vision systems. Global vision systems use single or multiple cameras positioned above the field's center to capture comprehensive field imagery. These systems apply algorithms to identify field objects, including robots, and collect accurate position data. This information then aids the robots' decision-making processes, such as pathway determination, guiding each robot in performing its tasks.

Visual extraction is crucial for robot navigation and task execution, especially for soccer robots requiring accurate positional data. Currently, visual extraction is grouped into three main types: traditional two-step extraction [1,2], camera self-extraction [3-8], and active vision-based extraction [9-12]. Zhang et al. [13] proposes traditional extraction necessitates precise extraction targets and multiple perspective images to

[1] Corresponding Author: Meiheng Zhang, meiheng5310@163.com

enhance accuracy, as seen in applications like Camera Extraction in Matlab [12] and extraction for an airport service robot. This method often requires extraction boards and specialized software, with strict requirements on the number of images and their spatial relationship to the camera, making it complex and time-intensive. Camera self-extraction uses nonlinear image constraints for extraction in unknown environments, relying on the camera's internal constraints. Active vision extraction requires specific camera movements, like translational motion, to determine internal parameters. Each method addresses different extraction needs and scenarios, maintaining references to the respective studies.

Global and autonomous visual system extraction for soccer robots has seen significant research. For global vision systems, Liu [14] employs a segmented linear model using specific feature points to solve for the parameter matrix. Dibs [15] uses polynomials to correct nonlinear geometric distortion, formulating equations from feature points' distorted and theoretical coordinates, with the least squares method determining polynomial parameters. A neural network modeling [16] the relationship between images and the actual field is discussed in detail and the mechanism is well constructed, while Hubara [17] achieves high extraction accuracy for a large-field robot using a two-step method starting from the camera imaging model. For autonomous systems, Tong [18] uses wavelet transform for heterogeneous binocular vision extraction, enabling ball trajectory's 3D reconstruction. Shi et al. [19] introduce a linear panoramic convex lens for capturing the environment, simplifying the extraction process by establishing a direct relationship between target image positions and actual field locations. Juang and Lee [20] extracts humanoid soccer robots using grid points on the field for self-positioning and obstacle distance estimation through gait counting and image analysis.

Low-Rank Trajectory Recovery (LRTR) methods, focusing on identifying a low-dimensional subspace to capture movement trajectories' intrinsic structure while filtering out outliers and noise, have gained significant attention for their effectiveness, especially in applications like table tennis athlete movement analysis. This approach offers substantial improvements to sports analytics practices. Pose estimation techniques based on non-negative matrix factorization are divided into matrix-based [21-23] and tensor-based [24-26] methods. Matrix-based methods treat pose data as a matrix, applying low-rank decomposition or factorization to learn the subspace. Tensor-based methods view image data as a tensor, employing decomposition or factorization techniques to uncover complex patterns with-in multidimensional data.

Despite the merits of LRTR in intelligent movement trajectories extraction, several unresolved issues require attention. A primary challenge involves the selection of optimal rank and sparsity parameters for the low-rank and sparse decomposition [22], which significantly impact the quality of the matrix and the features during trajectory extraction. Another hurdle is addressing the nonlinearity and heterogeneity inherent in trajectory data, which may not be accurately represented by a single linear matrix or a combination of multiple matrices. Additionally, incorporating prior knowledge of moving trajectory data, spectral information, or semantic information, into the LRTR framework to enhance the interpretability and applicability of features is a crucial concern.

Motived by the above analysis, this paper addresses the abovementioned challenges by proposing an improved LRTR method capable of adaptively determining the rank and sparsity parameters, exploiting the nonlinear and heterogeneous structure of recorded trajectory data, and integrating prior knowledge of trajectory data into the

overall evaluation and estimation process. This approach aims to assist the trajectory tracking process of soccer robots.

The rest of the paper is organized as follows: Section II gives the simplified establishment of extraction model, Section III analyzes and gives the internal and external parameter estimation of the simplified extraction model, Section IV provides the experimental result and Section V concludes the whole paper.

2. Background of Robust Principal Component Analysis (RPCA) and Utilization IN Camera Mapping

2.1. Background of Robust Principal Component Analysis (RPCA)

As illustrated in Figure 1, in the global vision system of soccer robots, the camera monitors the field from a fixed viewpoint, continuously capturing the pose information of robots. This data supports the decision-making system in adopting optimal processing strategies. Therefore, visual extraction is an essential prerequisite.

Figure 1. Soccer Robot Global Vision System

Robust Principal Component Analysis (RPCA) plays a crucial role in intelligent image feature extraction. By applying RPCA to image data, it effectively handles complex images characterized by noise, outliers, or variations. This technique is essential for improving the quality of image data in challenging scenarios, such as image that contains the movement information.

Robustness Handling: RPCA is engineered to manage image data encompassing noise, outliers, and variations. In the realm of intelligent image feature extraction, where real-world scenarios may introduce diverse disturbances and uncertainties, RPCA bolsters the robustness of algorithms, guaranteeing efficient feature extraction despite the presence of such disturbances.

Decomposition of Movement Image Components: RPCA can decompose a movement image into two matrices — one representing the main components with a low-rank structure and the other representing noise or outlier components with a sparse structure. This decomposition facilitates the extraction of essential feature information from the image while removing irrelevant noise for image analysis tasks.

Subspace Learning: RPCA explores the subspace structure of the image, enhancing the discriminative nature of feature extraction through principal component analysis on

image data. This is especially beneficial for discerning significant structures and patterns within images.

Movement Image Recovery: RPCA not only extracts valuable features but also possesses the ability to reconstruct the original movement features from a noisy or outlier-containing image. This enhances image quality and preserves essential movement information.

To provide a clearer depiction of the RPCA process, the flowchart of the Robust PCA algorithm is presented in Figure 2.

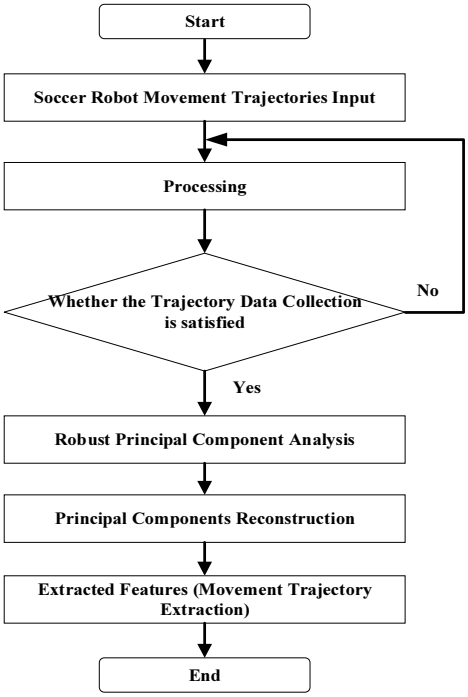

Figure 2. Flow chart of robust PCA algorithm in a typical trajectory extraction

2.2. RPCA based Camera Mapping

During the trajectory extraction process, the mapping relationship from the real-world coordinate system to the camera coordinate system for a spatial point is expressed by:

$$P_c = RP_w + T \tag{1}$$

In Eq. (1), R the rotation matrix is generally a 3×3 matrix with elements ranging from R_1 to R_9. Considering the complexity of solving, this rotation matrix is represented using Rx, R_Y, R_Z, and Euler angles, where the rotation can be expressed as Eq. (2). T is the translation matrix, with its three translation components being T_X, T_Y, and T_Z.

$$R = \begin{bmatrix} cR_z cR_y & sR_z cR_y & -sR_y \\ -sR_z cR_x + cR_z sR_y sR_x & cR_z cR_x + sR_z sR_y sR_x & cR_y sR_x \\ sR_z sR_x + cR_z sR_y cR_x & -cR_z sR_x + sR_z sR_y cR_x & cR_y cR_x \end{bmatrix} \tag{2}$$

Where $s = \sin(\cdot)$, $c = \cos(\cdot)$. Considering that the camera in the soccer robot global vision system is vertically mounted directly above the field, its optical axis is approximately perpendicular to the field plane. The imaging plane is nearly parallel to the field plane. Therefore, $R_x \approx 0$, $R_y \approx 0$. Thus, an approximation is applied to the rotation matrix. In the expression for the first row of the rotation matrix, $\cos R_y \approx 1$, $\sin R_y \approx R_y$. In the expression for the second row, $\cos R_x \approx 1$, $\cos R_y \approx 1$, $\sin R_y \approx 0$, $\sin R_x \approx R_x$. In the expression for the third row, $\cos R_y \approx 1$, $\cos R_x \approx 1$, $\sin R_y \approx R_y$, $\sin R_x \approx R_x$. The rotation matrix can be simplified as Eq. (3).

$$R' = \begin{bmatrix} \cos R_z & \sin R_z & -R_y \\ -\sin R_z & \cos R_z & R_x \\ R_x \sin R_z + R_y \cos R_z & -R_x \cos R_z + R_y \sin R_z & 1 \end{bmatrix} \tag{3}$$

Under this mapping relationship, there are six parameters to be solved: R_x, R_y, R_z, T_x, T_y, T_z. These are referred to as the camera external parameters.

Camera imaging can be viewed as the perspective projection of a pinhole camera. Based on its geometric relationship, the camera coordinates and ideal target surface coordinates have the following relationship:

$$\begin{cases} X_u = Z_c \dfrac{X_c}{f} \\ Y_u = Z_c \dfrac{Y_c}{f} \end{cases} \tag{4}$$

Due to the presence of distortion in the image, there is a certain transformation relationship between ideal target surface coordinates and distorted target surface coordinates. Typically, image distortion includes two types: radial distortion and tangential distortion. Each type of distortion can be represented by an infinite series. In camera extraction, only radial distortion is considered, and tangential distortion is ignored. Moreover, in the expression for radial distortion, only the first term of the infinite series is taken, i.e., the quadratic term. The specific expression is:

$$\begin{cases} D_x = X_d k_1 (X_d{}^2 + Y_d{}^2) \\ D_y = Y_d k_1 (X_d{}^2 + Y_d{}^2) \end{cases} \tag{5}$$

The relationship between ideal coordinates and distorted coordinates can be expressed as:

$$\begin{cases} X_u = X_d + D_x \\ Y_u = Y_d + D_y \end{cases} \tag{6}$$

Camera extraction aims to establish the correspondence between the world coordinate system and the image coordinate system. This is essential because it involves considering the transformation relationship between target surface coordinates and image coordinates. Typically, the distance from the center to the center of two pixels on the CCD photosensitive element is defined as dx in the horizontal direction and d_y in the vertical direction. During camera operation, the time difference between image acquisition hardware and scanning hardware, which cannot be perfectly synchronized, or inaccuracies in the camera's exposure time, introduce an uncertain image scale factor to mitigate hardware-related uncertainties. This paper focuses solely on the uncertain scale factor s_x in the X direction of the image, as the uncertainty in the Y direction can be resolved through the extraction of the focal length value. Therefore, a separate uncertain scale factor in the Y direction is not considered.

With the parameters set as above, the relationship between distorted target surface coordinates and image pixel coordinates can be expressed as:

$$\begin{cases} X_d = (X_f - C_x)d_x / S_x \\ Y_u = (Y_f - C_y)d_y \end{cases} \tag{7}$$

C_x and C_y represent the central coordinates of the image. When capturing at maximum resolution, the central coordinates of the image are exactly half of the resolution value. In cases where the camera captures within a Region of Interest (ROI), C_x and C_y must be determined as extraction parameters. By integrating Eq. (1) through (7), one can derive the transformation relationship between the image coordinates (X_f, Y_f) and the world coordinates (X_w, Y_w, Z_w). The specifics of this derivation are not elaborated here. It can be deduced that, throughout the extraction process, in addition to extracting six external parameters involving rotation and translation, there are also five internal parameters to solve: the focal length f, an uncertain scale factor s_x in the X direction of the image, the radial distortion coefficient k_1, and the pixel coordinates C_x, C_y at the intersection of the optical axis with the CCD imaging plane within the image coordinate system.

3. Proposed Low-Rank Trajectory Recovery (LRTR) Method and Optimization Algorithm

To effectively determine camera extraction parameters, acquiring a set of reference points within a real-world coordinate system is crucial. In this section, we propose low-rank trajectory recovery (LRTR) method, which is based on low-rank optimization, along with its associated optimization algorithm. LRTR is specifically designed to improve the robustness of feature extraction when dealing with noisy and diverse image data. The optimization algorithm is employed to ensure efficient learning of the subspace. The mathematical formulation of this process is delineated by the following equations:

The proposed LRTR: The LRTR method is formulated with the aim of capturing the robust subspace structure inherent in image data. The objective function is defined as follows in Eq. (8)

$$J(X,L,S) = \arg\min_L \sum_{i=1}^{n} \left\| X_i - L - S_i \right\|_F^2 + \lambda \left\| S_i \right\|_1 \tag{8}$$

where, X_i is the input image data,
L is the low-rank subspace,
S_i is the sparse noise,
$\|\cdot\|_F$ denotes the Frobenius norm,
λ is the regularization parameter.

Optimization Process: The optimization algorithm is employed to facilitate efficient convergence. It entails iterative steps aimed at updating both the low-rank subspace L and the sparse noise S_i. Following each iteration, the optimization process can be succinctly expressed as follows:

$$\begin{aligned} &\min_{L,Z,S} \sum_{i=1}^{n} \left\| L \right\|_* + \lambda \left\| S_i \right\|_1 \\ &\text{s.t. } X\text{diag}(Z)=L+S, \quad \forall k \in [k],\ 1^T Z^{(K)} = 1 \end{aligned} \tag{9}$$

While explicit enforcement of non-negativity upon variable Z is not mandatory, the optimal solution derived from the aforementioned program consistently ensures $Z \geq 0$, as corroborated by the subsequent theorem. This phenomenon stems from the unique advantageous characteristics exhibited by the nuclear norm and $\ell 1$ norm. Such properties prove exceptionally advantageous for this particular problem, especially considering that the efficiency of the proposed algorithm utilizing the Augmented Lagrangian Method diminishes swiftly with an increase in the number of constraints. This observation obviates the necessity of appending an additional N inequality constraint to the convex program.

Theorem 1: In the event that none of the columns of matrix X equals zero, the optimal solution denoted as Z^* in Eq. (9) will remain non-negative.

Proof Suppose an optimal solution (A, L, S) can be satisfied when S has negative entries. Then it can be assumed that the triple ($\hat{A}$, $\hat{L}$, $\hat{S}$) constructed in the following way:

$$\begin{aligned} \hat{Z}^{(k)} &= \frac{1}{1^T \left| Z^{(k)} \right|} \left| Z^{(k)} \right| \\ \hat{L}^{(k)} &= \frac{1}{1^T \left| Z^{(k)} \right|} L^{(k)} \text{diag}\left[\text{sign}(Z^{(k)}) \right] \\ \hat{S}^{(k)} &= \frac{1}{1^T \left| Z^{(k)} \right|} S^{(k)} \text{diag}\left[\text{sign}(Z^{(k)}) \right] \end{aligned} \tag{10}$$

Where the ^ means the estimated value, sign(·) is the signum function and its expression is:

$$\text{sign}(i)=\begin{cases}1 & \text{if } i>0\\ 0 & \text{if } i=0\\ -1 & \text{if } i<0\end{cases} \tag{11}$$

After the optimization, the RSL is able to decompose a data matrix $X \in \mathbb{R}^{m\times n}$, into low-rank ($L \in \mathbb{R}^{m\times n}$) and sparse ($S \in \mathbb{R}^{m\times n}$), components, capturing main structures and outliers, respectively.

$$\mathcal{L}(L,S_i,Y_i,\mu)=\left|L\right|_* + \lambda\left|S\right|_1 + \left\langle Y_i, X_i - L - S_i\right\rangle + \frac{\mu}{2}\left\|X_i - L - S\right\|_F^2 \tag{12}$$

where, L, S_i are the low-rank and sparse components,
Y is the Lagrange multiplier,
μ is the Penalty parameter,
$\langle \cdot,\cdot \rangle$ is the inner product,
$\|\bullet\|_F$ denotes the Frobenius norm.
The IALM update rules are as follows:
1) Update L^{k+1}:

$$L^{k+1} = \mathcal{D}_{\frac{1}{\mu^k}}\left(X - S^k + \frac{Y^k}{\mu^k}\right)$$

2) Update S^{k+1}:

$$S^{k+1} = \mathcal{S}_{\frac{1}{\mu^k}}\left(X - L^k + \frac{Y^k}{\mu^k}\right),$$

3) Update Y^{k+1}:

$$Y^{k+1} = Y^k + \mu^k\left(X - L^k - S^{k+1}\right),$$

4) Update μ^{k+1}

$$\mu^{k+1} = \rho\mu^k.$$

The operation definitions are as follows:

$$\begin{aligned}&\mathcal{D}\alpha(Z) = \mathcal{D}U\mathcal{S}\alpha(\Sigma)V^T\\ &\mathcal{S}_\alpha(Z) = \text{sign}(Z)\odot\max\left(\left|Z\right|-\alpha,0\right)\end{aligned} \tag{13}$$

As for convergence concern, the IALM converges to the optimal RPCA solution results under mild conditions.

4. Experimental Results

This section provides a thorough verification of the proposed algorithm (LRTR and its optimization method) for soccer robot movement trajectories extraction, together with the comparison of already existed methods.

4.1. Algorithm Implementation and Software Configuration

The trajectory data collection process of soccer robot target on the field is shown in Figure. 3. The movement extraction process for the vision system of the MiroSot 5:5 soccer robot is carried out based on the pre-designed model parameters. The dimensions of the playing field are 240cm×180cm. The system employs a Basler A312fc 1394 camera with a Tamron 12VM412ASIR manual zoom lens. The distance from the lens to the field is approximately 2.5m, and the image resolution is 640×480 pixels. The initial values of C_x and C_y are estimated to be at the image centre (320,240).

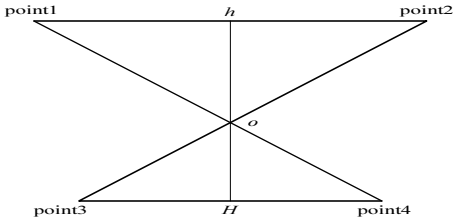

Figure 3. Illustration of initial focal length estimation

4.2. Trajectory Extraction and Solving Parameters Configurations

Due to the requirements of the soccer robot vision system for the trajectory extraction process to be easy to operate and quickly implementation, using standard extraction process such as chessboards can improve accuracy but makes the process cumbersome. Moreover, the control system requires extraction accuracy to reach the millimetre level to meet the control requirements. Therefore, inherent landmarks on the field are used as representatives of the soccer robot. The distribution of target points on the field is shown in Figure. 4, and their image coordinates are manually obtained. World coordinates can be obtained based on the established world coordinate system and the spatial relationships of the target points on the field. According to the above movement extraction model, the results of the extraction calculation for intrinsic and extrinsic soccer robot parameters are shown in Table 1 and Table 2, respectively.

Figure 4. Distribution of soccer robots on the field

Table 1. Soccer Robots External Parameter Extraction Results

External Parameter	Extraction Results
R_X (rad)	0.125678
R_y (rad)	-0.234567
R_Z (rad)	-2.34567
T_x (cm)	145.6789
T_y(cm)	88.901234
T_z (cm)	-215.789

Table 2. Soccer Robots Internal Parameter Extraction Results

Internal Parameter	Exraction Results
f (mm)	6.047536
C_x (pixels)	333.925904
C_y (pixels)	243.412431
s_x	5.999321
k_1	-6.992488

4.3. Trajectory Extraction Error Comparison Analysis

Utilizing the solved parameters, the field image undergoes distortion correction first. Figure. 5 displays the original field image, exhibiting noticeable barrel distortion due to the use of a wide-angle lens in the vision system.

Figure 5. Original site image

After applying the correction method to correct the coordinates of the original field image, the corrected field, depicted in Figure. 6, demonstrates effective correction of the barrel distortion.

Establishing the lower left corner of the field border as the origin of the world coordinate system, with the direction horizontal to the right and the *Y* direction vertical upwards. When the ball is tightly against the lower border of the field, the diameter of the ball is 42.7 mm, and its theoretical *Y*-coordinate value is 21.35 mm. Take 20 sampling points along the lower border of the field, accurately extract the coordinates of the sampling points using the simplified two-step method proposed in this paper, and compare them with the polynomial fitting method and the piecewise linear movement

extraction method. The results, as shown in Figure. 7, indicate that the movement trajectory extracted by the simplified two-step method are closer to the theoretical true values compared to the other two methods. Through the comparison analysis of the absolute error values shown in Figure. 8, it can be concluded that the maximum absolute error value of the simplified two-step method is approximately 1 millimetre, with an average absolute error value of 0.877 mm; the maximum absolute error value of the polynomial fitting method is about 3 mm, with an average absolute error value of 2.144 mm; and the maximum absolute error value of the piecewise linear method is about 6 mm, with an average absolute error value of 3.312 mm.

Figure 6. Converted site image

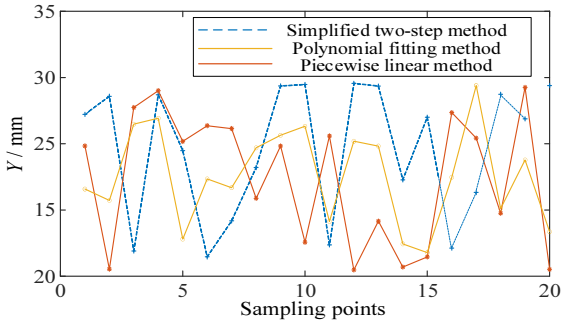

Figure 7. Comparison of results corresponding to different extraction methods

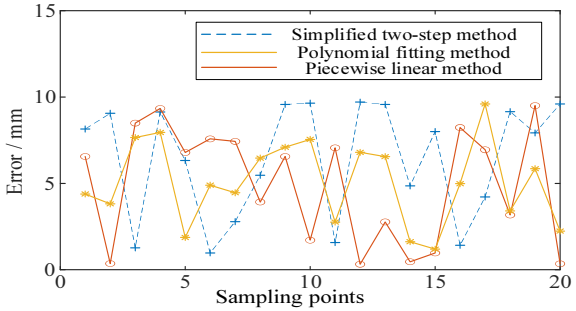

Figure 8. Comparison of errors corresponding to different extraction methods

Table 3. Robot Movement Extraction Test

Extraction Method	Number of Tests	Success Count	Success Rate
Piecewise Linear Method	85	56	66%
Polynomial Fitting	85	75	88%
Simplified Two-Step Method	85	80	95%
Proposed Method	85	83	98%

One of the most common strategies in soccer robot systems is robot shooting, where robots need to predict the trajectory of the ball to complete flanking shots and score goals. Whether the robot can eventually complete the shooting action and score is

directly related to the prediction of the ball's trajectory. The prediction of the ball's trajectory is directly related to the extraction results of the visual system. Therefore, for the afore-mentioned robot actions, tests were conducted on visual systems extracted using piecewise linear, polynomial fitting, and simplified two-step methods. The test results are shown in Table 3. Experimental results demonstrate that using the simplified two-step method can improve the movement trajectory extraction accuracy of the soccer robot.

5. Conclusion

This paper explores a visual detection and tracking system tailored for a soccer robot, beginning with a comprehensive description of an Enhanced Low-Rank Trajectory Recovery method. This method constructs the trajectory extraction model and facilitates the determination of both internal and external parameters essential for optimization. Using the refined extraction model, we derive a methodology for solving these parameters. To ensure precision in parameter adjustment, a stepwise optimization technique is employed to achieve the best possible outcomes. Furthermore, we calibrate and validate the Mirosof 5:5 soccer robot vision system. The calibration process involves manual traction for extracting reference points on the field, which assists in determining the camera's internal and external parameters. Experimental findings confirm the high accuracy of our simplified two-step method, achieving an extraction precision of ±1 mm. When compared to traditional methods such as segmented linear and polynomial fitting, our approach provides superior extraction accuracy, thereby satisfying the stringent control demands of the robot's decision-making system.

The future work of this paper will focus on the exploration of image processing methods for automatically obtaining image coordinates of calibration reference points on the field, achieving higher subpixel accuracy, and further improving the accuracy of system calibration ability.

References

[1] Lee G, Kim W, Oh H. Review of statistical model calibration and validation—from the perspective of uncertainty structures. Structural and Multidisciplinary Optimization, 2019, 60: 1619-1644.
[2] Li S, Li X, Chen S. Two-Step LiDAR/Camera/IMU spatial and temporal calibration based on continuous-time trajectory estimation. IEEE Transactions on Industrial Electronics, 2023, 3(2): 88-96.
[3] Merras M, El Hazzat S, Bouazi A. Camera self-calibration with varying parameters based on planes basis using particle swarm optimization. The Visual Computer, 2023, 39(7): 3109-3122.
[4] Cramariuc A, Petrov A, Suri R. Learning camera miscalibration detection. 2020 IEEE International Conference on Robotics and Automation (ICRA). IEEE, 2020: 4997-5003.
[5] Li Y, Zhao Z, Chen Y, et al. Automatic roadside camera calibration with transformers. Sensors, 2023, 23(23): 1355-1386.
[6] Gil Y, Elmalem S, Haim H, et al. Online training of stereo self-calibration using monocular depth estimation. IEEE Transactions on Computational Imaging, 2021, 7: 812-823.
[7] Ettalibi A, Elouadi A, Mansour A. AI and Computer Vision-based Real-time Quality Control: A Review of Industrial Applications. Procedia Computer Science, 2024, 231: 212-220.
[8] Li S, Yoon H S. Enhancing Camera Calibration for Traffic Surveillance with an Integrated Approach of Genetic Algorithm and Particle Swarm Optimization. Sensors, 2024, 24(5): 1456.
[9] Dai Z, Song H, Liang H, et al. Traffic parameter estimation and control system based on machine vision[J]. Journal of Ambient Intelligence and Humanized Computing, 2020: 1-13.

[10] Stoppa F, de Austri R R, Vreeswijk P, et al. AutoSourceID-FeatureExtractor-Optical image analysis using a two-step mean variance estimation network for feature estimation and uncertainty characterisation. Astronomy & Astrophysics, 2023, 680: A108.
[11] Li H, Jia P, Li W, et al. Towards Efficient Universal Adversarial Attack on Audio Classification Models: A Two-Step Method. International Symposium on Emerging Information Security and Applications. Singapore: Springer Nature Singapore, 2023: 20-37.
[12] Van Crombrugge I, Penne R, Vanlanduit S. Extrinsic camera calibration for non-overlapping cameras with Gray code projection. Optics and Lasers in Engineering, 2020, 134: 106305.
[13] Zang L, Zhang K, Tian C, et al. Three-dimensional Spatial Localization Based on Binocular Vsion. 2021, 187: 106425.
[14] Liu C, Zhi Z, Zhao W, et al. Research on Local Fingerprint Image Differential Privacy Protection Method Based on Clustering Algorithm and Regression Algorithm Segmentation Image. IEEE Access, 2024, 8(1): 1-5.
[15] Dibs H, Mansor S, Ahmad N, et al. Geometric correction analysis of highly distortion of near equatorial satellite images using remote sensing and digital image processing techniques. Engineering, 2022, 14(01): 1-8.
[16] Pranav E, Kamal S, Chandran C S, et al. Facial emotion recognition using deep convolutional neural network. 2020 6th International conference on advanced computing and communication Systems (ICACCS). IEEE, 2020: 317-320.
[17] Hubara I, Nahshan Y, Hanani Y, et al. Accurate post training quantization with small calibration sets. International Conference on Machine Learning. PMLR, 2021: 4466-4475.
[18] Tong C. Three-dimensional reconstruction of the dribble track of soccer robot based on heterogeneous binocular vision. Journal of Ambient Intelligence and Humanized Computing, 2020, 11(12): 6361-6372.
[19] Shi Y, Ying X, Zha H. Unsupervised domain adaptation for semantic segmentation of urban street scenes reflected by convex mirrors. IEEE Transactions on Intelligent Transportation Systems, 2022, 23(12): 24276-24289.
[20] Juang L H. Humanoid robots play chess using visual control. Multimedia Tools and Applications, 2022, 81(2): 1545-1566.
[21] Sadiq M T, Yu X, Yuan Z, et al. A matrix determinant feature extraction approach for decoding motor and mental imagery EEG in subject-specific tasks. IEEE Transactions on Cognitive and Developmental Systems, 2020, 14(2): 375-387.
[22] Li X, Leung F H F, Su S, et al. Sleep Apnea Detection Using Multi-Error-Reduction Classification System with Multiple Bio-Signals. Sensors, 2022, 22(15): 5560.
[23] Li C, Peng Y, Su M, et al. GPU parallel implementation for real-time feature extraction of hyperspectral images. Applied Sciences, 2020, 10(19): 6680-6695.
[24] Yuan L, Li C, Cao J, et al. Rank minimization on tensor ring: an efficient approach for tensor decomposition and completion. Machine Learning, 2020, 109: 603-622.
[25] Prasath S, THANH D N H. Structure tensor adaptive total variation for image restoration. Turkish Journal of electrical engineering and computer sciences, 2019, 27(2): 1147-1156.
[26] Wang Q, Gu Y. A discriminative tensor representation model for feature extraction and classification of multispectral LiDAR data. IEEE Transactions on Geoscience and Remote Sensing, 2019, 58(3): 1568-1586.